ACS NANO
Cite This: ACS Nano 2018, 12, 82–88
www.acsnano.org

ARTICLE

Broadband Photonic Spin Hall Meta-Lens

Junxiao Zhou,[†,∥] Haoliang Qian,[‡,∥] Guangwei Hu,[§] Hailu Luo,[*,†] Shuangchun Wen,[†] and Zhaowei Liu[*,‡]

[†]Key Laboratory for Micro-/Nano-Optoelectronic Devices of Ministry of Education, School of Physics and Electronics, Hunan University, Changsha 410082, China

[‡]Department of Electrical and Computer Engineering, University of California, San Diego, 9500 Gilman Drive., La Jolla, California 92093, United States

[§]Department of Electrical and Computer Engineering, National University of Singapore, 4 Engineering Drive 3, Singapore 117576, Singapore

Supporting Information

ABSTRACT: **Meta-lens represents a promising solution for optical communications and information processing owing to its miniaturization capability and desirable optical properties. Here, spin Hall meta-lens is demonstrated to manipulate photonic spin-dependent splitting induced by spin−orbital interaction in transverse and longitudinal directions simultaneously at visible wavelengths, with low dispersion and more than 90% diffraction efficiency. The broadband dielectric spin Hall meta-lens is achieved by integrating two geometric phase lenses with different functionalities into one single dynamic phase lens, which manifests the ultracompact, portable, and polarization-dependent features. The broadband spin Hall meta-lens may find important applications in imaging, sensing, and multifunctional spin photonics devices.**

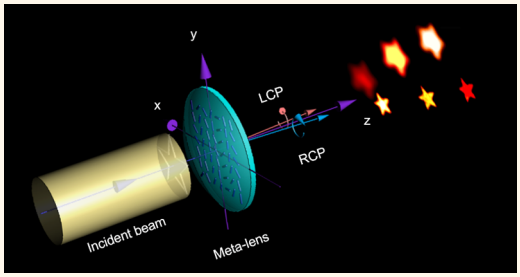

KEYWORDS: *meta-lens, geometric phase, dynamic phase, spin-dependent splitting, spin-dependent focusing*

Photonic spin Hall effect (PSHE) describes a transport phenomenon with optical spin-dependent splitting. It was theoretically predicted and proposed by Onoda *et al.* in 2004,[1] which is a counterpart of spin Hall effect in electron transport.[2] The root cause of the PSHE is generally regarded as an effective spin−orbital interaction, which is the interplay of spin and trajectory of the light beam. In light of the above theoretical studies, increasing efforts are made to experimentally investigate the PSHE.[3−9] However, it is difficult to measure this induced spin-dependent shift without weak measurement technology[3] or multiple reflections[4] because of the extremely small photon momentum and spin−orbit interaction. Recently, metasurface or metamaterial of reduced dimensionality makes it possible to direct and manipulate the electromagnetic field.[10−21] Interestingly, metasurface is also able to greatly enhance the spin−orbital interaction, because of its rapidly varying dynamic phase discontinuity, which can sharply change the light trajectory and, consequently, generate the spin-dependent geometric phase. Enormous investigations on experimental observation of the PSHE have been carried out based on the metasurface.[22−27] These developments enable the possibility for the applications of PSHE, such as precision metrology[28] and spin-based photonic devices.[29]

To date, however, major research efforts have been restricted on the single dimensional modulation including transverse or longitudinal spin-dependent splitting. The realization of multidimensional spin-dependent splitting is still a challenge by a single device, because neither a single pure dynamic nor a geometric phase element can simultaneously gain transverse and longitudinal phase gradients, which is the key of photonic spin-dependent splitting. However, it is known that geometric phase element can be employed to achieve the transverse spin-dependent splitting,[30−34] while the dynamic phase element provides the possibility for realizing the longitudinal spin-dependent splitting.[35] Therefore, we propose to integrate both dynamic and geometric phase elements to obtain a broadband photonic spin Hall meta-lens (PSHM) and generate multi-dimensional spin-dependent splitting in free space simultaneously.

We experimentally verify the spin-dependent splitting for visible wavelengths and investigate the normalized Stokes parameter S_3 that demonstrates the degree of circular-polarized character of the electromagnetic wave. The experimental results are consistent with the theoretical prediction that the spin-dependent splitting can be achieved in both transverse and longitudinal directions. Our finding provides extra degrees of freedom to control spin photonics and is potentially useful for exploiting multifunctional spin photonics devices.

Received: October 17, 2017
Accepted: December 6, 2017
Published: December 6, 2017

DOI: 10.1021/acsnano.7b07379
ACS Nano 2018, 12, 82–88

Figure 1a describes the schematic drawing of the spin-dependent splitting in transverse and longitudinal directions.

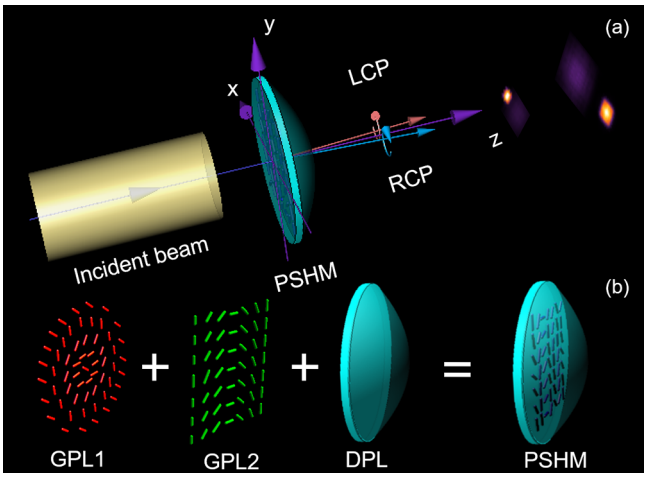

Figure 1. Illustration of multidimensional control of photonic spin Hall meta-lens. (a) The transverse and longitudinal spin-dependent splitting. RCP, right-handed circularly polarized light; LCP, left-handed circularly polarized light; GPL, geometric phase lens; DPL, dynamic phase lens; PSHM, broadband spin Hall meta-lens. (b) This lens is designed by integrating two geometric phase lenses (GPL1 and GPL2) with different functionalities on a dynamic phase lens (DPL).

When the PSHM is normally illuminated with a linearly polarized Gaussian light beam, it generates the desired continuous local phase profile for the two transmitted beam components which consist of two opposite helicity states corresponding to the left- and right-handed circularly polarized components, respectively. After the PSHM, left- and right-handed circularly polarized beams propagate toward different directions and are focused at different lengths, which corresponds to the desired longitudinal spin-dependent splitting. As shown in Figure 1b, the PSHM in this work is designed by integrating two different functional geometric phase lenses into a dynamic phase lens.

Let us briefly analyze the geometric phase, which is also known as Pancharatnam–Berry phase. It is not introduced by optical path difference, but results from the space-variant polarization manipulation.[36,37] The geometric phase elements use this characteristic to obtain the desired phase front, which is polarization dependent, notably unlike a conventional optical element.[38] The desired PSHM is attained by designing slabs with the effective optical axes of which the orientation angles θ are spatially modulated. Its space-variant local optical axes are a combination of the two geometric phase lenses axes, as depicted in Figure 2a–c. Note that the transverse and longitudinal spin-dependent splittings are led by the phase gradient in the respective directions. It can be written as

$$\theta = \theta_1 + \theta_2 = \frac{\pi}{2}\left(\sqrt{x^2 + y^2 + f_1^2} - f_1\right) + \frac{\pi x}{\Lambda} \quad (1)$$

The first part θ_1 with f_1 = 200 mm being the focal length of the lens is employed to focus one spin component and defocus the other, as shown in Figure 2a. The second part θ_2 is depicted in Figure 2b with the period Λ = 0.1 mm, which yields to a linear phase as a result of generating transverse spin-dependent splitting. It is similar to "catenary of equal phase gradient" reported in a previous reference.[39] Note that both phases

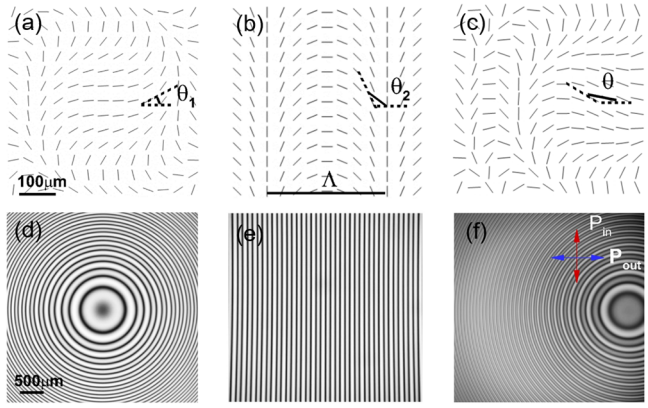

Figure 2. Illustration of the concept of PSHM by utilizing the space-variant geometrical phase. (a–c) Two-dimensional slow-axis orientation map of GPL1 (a), GPL2 (b), and PSHM (c). (d–f) Two-dimensional slow-axis orientation map of GPL1 (d), GPL2 (e), and PSHM (f). (d–f) Polariscopic analysis carried out by optical imaging between crossed linear polarizers under incoherent spatially extended illumination at a wavelength of 633 nm. P_{in} and P_{out} denote the input and output polarization states of light.

generated by the two parts θ_1 and θ_2 are geometric phases in nature. The Pancharatnam–Berry phases can be written as $\Phi_1 = 2\sigma_{\pm}\theta_1$ and $\Phi_2 = 2\sigma_{\pm}\theta_2$, where $\sigma_{\pm}$ = +1 and −1 denote left-handed and right-handed circular polarization.

To prove our concept, a sample is made by form-birefringent nanostructured glass slabs (Altechna R&D). Such a sample was fabricated by femtosecond laser writing of spatially varying nanostructures in a fused silica glass, and the induced form-birefringence patterns can be achieved by changing the writing parameters.[40] The nanostructures are at a deep subwavelength scale, thus can be treated as uniform media. At every point of the written area, the local optical axis is oriented parallel and perpendicular to the nanostructures, which leads to an artificial uniaxial crystal (also see the Methods section for details). Here, we examine polariscopic optical characterization images to characterize the induced space-variant birefringence patterns embedded in the silica glass.[41] The crossed linear polarizer images of the prepared sample at a wavelength of 633 nm are displayed in Figure 2d–f, which are summarized in the polariscopic optical characterization images of GPL1, GPL2, and PSHM. The off-centered series of concentric rings in Figure 2f suggests that the orientation of local optical axis changes along the transverse and longitudinal directions.

To get an insight of the microscopic structure of the PSHM device, the sample was cut though the patterned area and polished. The photographs in Figure 3a,b show that the PSHM was embedded inside of the glass slide. The series of concentric rings (inset of Figure 3a) corresponds to the crossed linear polarizers image in the Figure 2f. The dark-field optical image (see Figure 3c) reveals that the laser written layer has a thickness about 80 μm. The SEM image in Figure 3d further confirms that the laser exposure formed some self-assembled vertically aligned nanostructures at deep subwavelength scales, approximately 30–90 nm.

The phase Φ introduced by the PSHM can be further combined with a dynamic phase lens (DPL), so that the total phase of the PSHM is expressed as follows

DOI: 10.1021/acsnano.7b07379
ACS Nano 2018, 12, 82–88

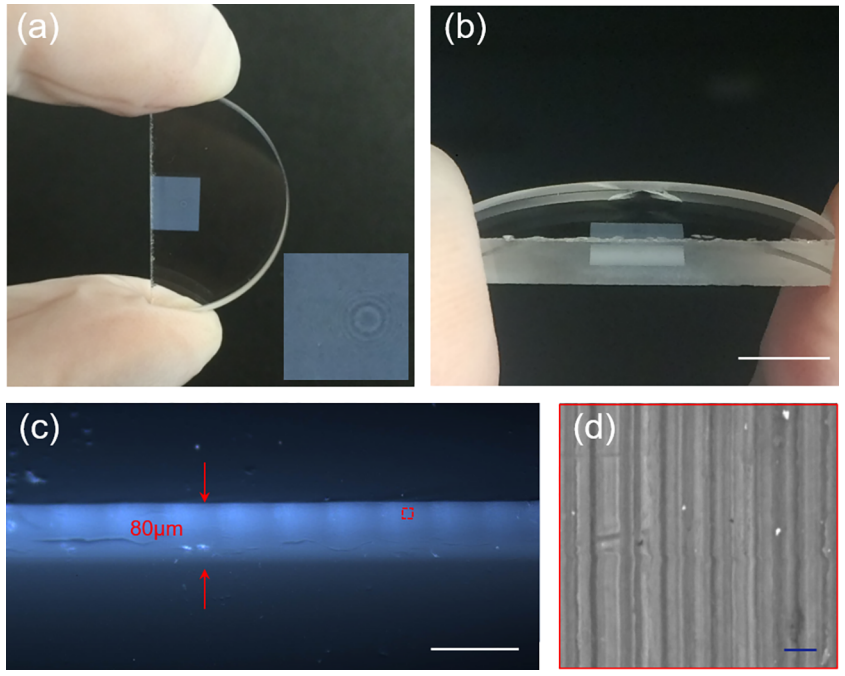

Figure 3. (a) Top-view photograph of the PSHM. Inset: Zoomed-in view shows the center patterned area of the sample. (b) Side-view photograph of the sample. Scale bar is 4 mm. (c) The dark-field microscopy image for the cross-section of the PSHM sample reveals microscopic laser written patterns. Scale bar 100 μm. (d) Zoomed-in SEM image of the boxed area in (c). Scale bar is 300 nm.

$$\Phi = \Phi_1 + \Phi_2 + \Phi_3 = \frac{2\pi}{\lambda}\left(\sqrt{x^2 + y^2 + f_1^2} - f_1\right) + \frac{2\pi x}{\Lambda} + \frac{\pi}{\lambda}\left(\frac{x^2 + y^2}{f_2}\right) \quad (2)$$

where f_2 = 125 mm is the focal length of a DPL in this specific case. Figure 4 summarizes the phase introduced by GPL1, GPL2, DPL, and PSHM under the illumination of left- and right-handed circularly polarized light. GPL1 can be regarded as an ultrathin convex/concave lens, for left/right-handed polarization, respectively. This PSHM is a combination of an ultrathin convex/concave lens, GPL2 and DPL.[42] Therefore, the focal length of the PSHM can be calculated as

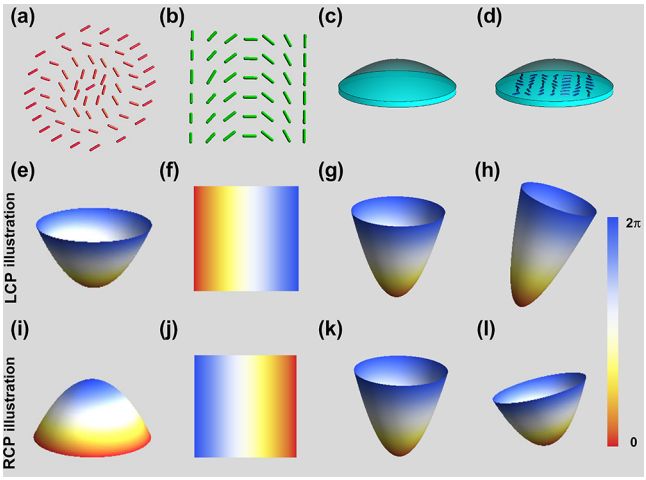

Figure 4. Phase introduced by GPL1, GPL2, DPL, and PSHM in order from left to right. The second and third rows refer to left-handed circularly polarized light (LCP) and right-handed circularly polarized light (RCP), respectively.

$$f_{\sigma_\pm} = \frac{f_1 \times f_2}{f_1 + \sigma_\pm f_2} \quad (3)$$

One circular handedness focuses at $f_{\sigma_-} = f_1 \times f_2/(f_1 + f_2)$ = 77 mm, while the orthogonal handedness has an apparent focal length of $f_{\sigma_+} = f_1 \times f_2/(f_1 - f_2)$ = 333 mm.

In Figure 4, with the phase modulation of GPL2 in PSHM, the two spin components will obtain two mutually conjugated tilted phases and separate transversely with each other during the propagation. The transverse spin-dependent splitting arises from the modulation of the geometric phase $\sigma_\pm\Phi_2$, which will induce a spin-dependent momentum shift occurring in x direction, $\Delta k_x = -2\sigma_\pm(\pi/\Lambda)$.[30] Therefore, the real-space shift caused by the momentum shift with the propagation distance z can be given as[43]

$$\Delta x = \frac{\Delta k_x}{k_0} Z = -\sigma_\pm \frac{\partial \Phi_2}{\partial x} Z = -\sigma_\pm \lambda Z/\Lambda \quad (4)$$

where $k_0 = 2\pi/\lambda$ denotes the vacuum wave vector. Note that Δk_x is a spin-dependent transverse momentum shift, that is, an angular shift. Combined with eq 3, the coordinates of the two focuses should be $(\sigma_-\lambda f_{\sigma_+}/\Lambda, 0, f_{\sigma_+})$ and $(\sigma_+\lambda f_{\sigma_-}/\Lambda, 0, f_{\sigma_-})$, which is (−0.487 mm, 0 mm, 77 mm) and (2.107 mm, 0 mm, 333 mm) in our exemplary design with f_1 = 200 mm, f_2 = 125 mm, and Λ = 0.1 mm.

RESULTS AND DISCUSSION

The PSHM is illuminated with a linearly polarized Gaussian beam at the 633 nm wavelength (17 mW, Thorlabs HNL210L-EC). The xz plane horizontal plot in the bottom of Figure 5 clearly demonstrates the evolution characteristics of the spin-dependent splitting and focusing. The output beam transversely

DOI: 10.1021/acsnano.7b07379
ACS Nano 2018, 12, 82−88

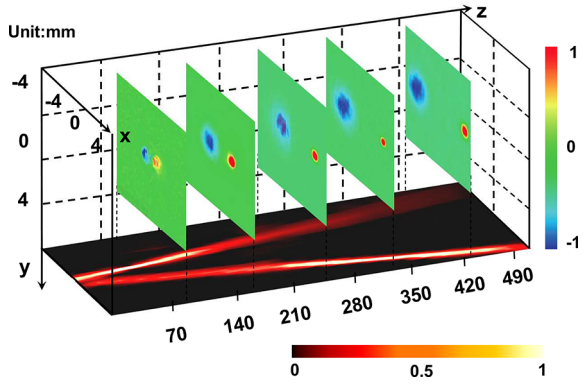

Figure 5. Experimentally measured beam propagation profile after the PSHM. The five vertical slices display normalized Stokes parameter S_3 of the beams at the planes where z is equal to 77, 160, 245, 333, and 430 mm. The horizontal plot shows the evolution characteristics of the spin-dependent splitting.

splits into left- and right-handed components after the PSHM, experiencing two distinct focuses, respectively. Further, for describing the spin (circular polarization degree) of the output electric field, a quarter-wave plate and a linear polarizer are set in sequence behind the PSHM for measuring the S_3.[44] The five vertical slices in Figure 5 display the far-field normalized Stokes parameter S_3, where the blue and red denote to the left- and right-handed circular polarizations, respectively.

In order to achieve similar performance for multiple wavelengths, nanoresonator-based meta-lens need to be specially designed due to its strong dispersive nature.[45] In our work, PSHM can be operated over a broadband wavelength range based on the characteristic of small dispersion across the whole visible spectrum. Figure 6a–j shows the experimentally measured results of the spin-dependent splittings in green (510 nm) and blue (430 nm) frequencies. All results are obtained from the same device as done for 633 nm. It can be easily seen that for all measured wavelengths here, the device shows that two spin-dependent focusing points arise at different positions with opposite transverse shifts, displaying the broadband behavior of the PSHM. The three colors are randomly selected without any specific design.

One of the significant parameters which can be utilized to evaluate the performance of our device is the diffraction efficiency, defined as $\eta = \frac{P_{LCP} + P_{RCP}}{P_{LCP} + P_{RCP} + P_0}$, where P_{LCP}, P_{RCP}, and P_0 are the output power of LCP, RCP, and zero-order components, respectively. The measured diffraction efficiencies by a laser power meter in the experiment are approximately 91.5%, 96.9%, and 96.8% at wavelengths of 430, 510, and 633 nm. The corresponding transmission efficiencies (the ratio between the transmitted power and the incident power) are as high as 88.9%, 91.2%, and 93.4%. Note that a broadband metasurface achieved by the suppression of chromatic aberration is proposed, which works at an infrared wavelength with a lower efficiency.[46] Thus, from the practical point of view, the PSHM in this work may be an excellent candidate for optical integration in a compact and efficient assembly based on its optical properties. The PSHM is compatible with the conventional optical element, since they are both completely made by glass.

Owing to the low loss and broadband properties, the developed device might find various applications in the optical imaging field.[47] To demonstrate the polarization-dependent

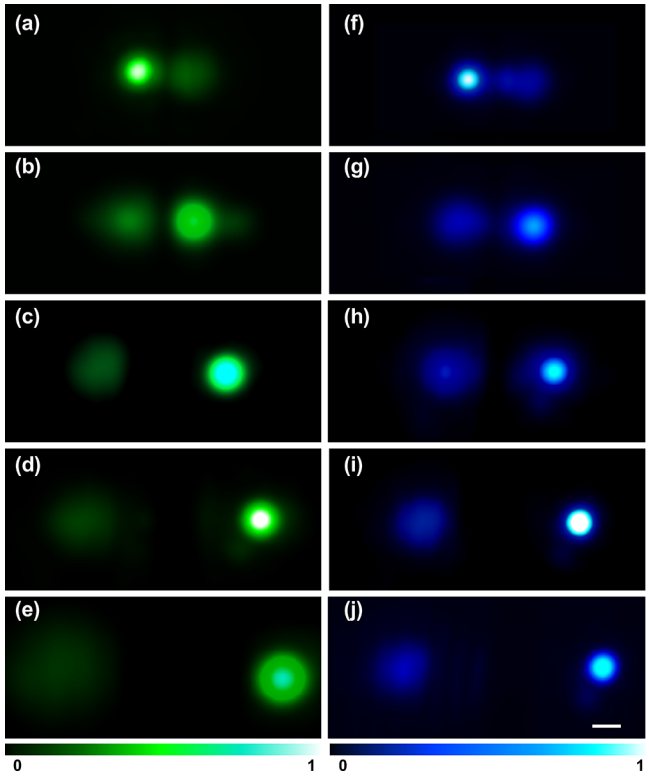

Figure 6. Experimentally measured results of photonic spin-dependent splitting. The wavelengths of the incident light are (a–e) 510 nm and (f–j) 430 nm, respectively. The normalized intensity distributions are measured at the distances of 77, 160, 245, 333, and 430 mm. Scale bar: 500 μm.

imaging of our device, the illumination beam is incident on a spatial light modulator (Holoeye LC-2012) loaded with a shape of a star. The light transmitted from the spatial light modulator passes through a quarter-wave plate, which is employed to tune the polarization property of the light (details in the Supporting Information). During the experiment, one of the two focuses ($f_{\sigma_\pm}$ = 333 mm) is chosen to form the image as an example. The spatial light modulator, which acted as an object, is placed 160 cm before the PSHM device. According to the lens imaging formula, the CCD camera is fixed at the image plane, that is, 420 mm after the PSHM.

We rotate the quarter-wave plate to change the incident light polarization type and record the corresponding images by the CCD camera at the same location. As shown in the top row of Figure 7, the right-handed incident light only forms an inverted and bright image, in the dashed circle on the right side. The intensity of that image gradually diminishes when the quarter-wave plate changes the incident light from right-handed polarization to left-handed polarization. Meanwhile, the off-focused image for the left-handed component gradually increases intensity to its maximum. The shown images are recorded at the wavelengths of 633, 510, and 430 nm, respectively. As expected, Figure 7 shows that the intensity of star images can be transferred between the two spin components by rotating the quarter-wave plate, and different wavelengths show the similar performance.

CONCLUSION

In summary, by employing a high-efficient diffraction device PSHM and applying the spin–orbit interaction mechanism, the

DOI: 10.1021/acsnano.7b07379
ACS Nano 2018, 12, 82–88

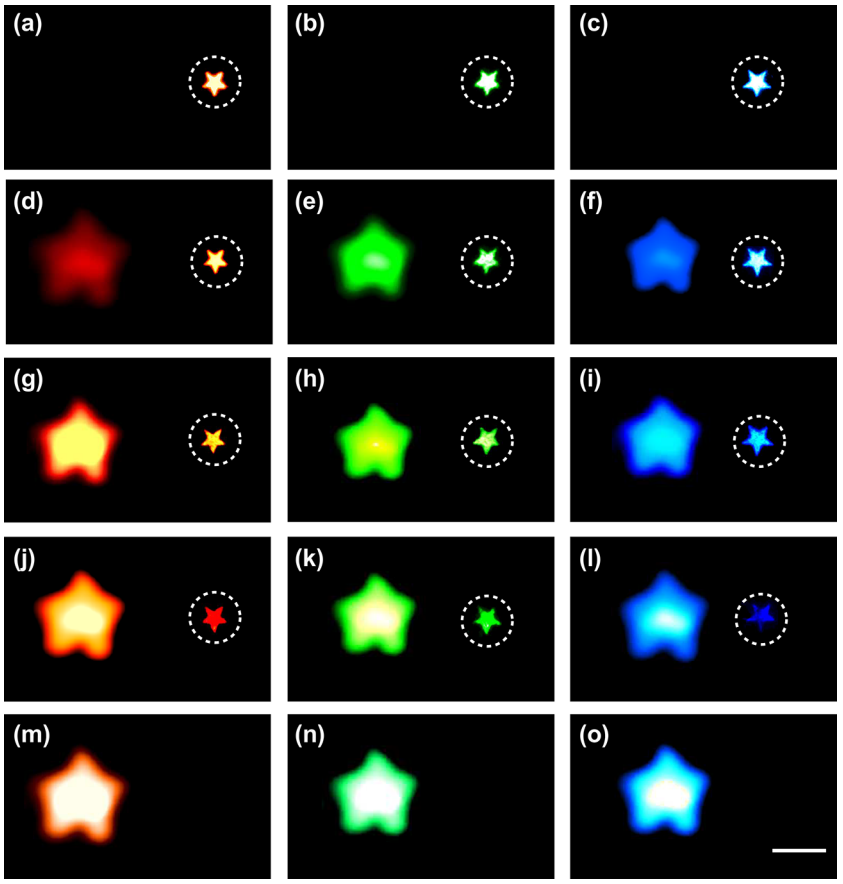

Figure 7. Recorded star images at different wavelengths. Different types of polarized incident light impinge the meta-lens for tuning the intensity of the image. The first, second, and third columns are measured at the same propagation distance under 633, 510, and 430 nm wavelengths illumination. Scale bar: 2 mm.

multidimensional spin-dependent splitting has been proposed and demonstrated, which provides one more degree of freedom in manipulating photons. For example, the spin-dependent meta-lens can be combined with two independent detectors to simultaneously retrieve the polarization state of the incident beam with very limited form factor. Our approach to designing PSHM enables the feature to generate spin-dependent splitting, focusing, and imaging. The presented design method provides an optical device with features of miniaturization and circular polarization dependence. The optical integration concept of designing geometric phase elements circumvents the limitations of bulky optical devices in conventional integrated optics. It has a significant impact on multifunctional optical elements and drastically increases the functionality density of the optical system. The polarization-dependent imaging properties emphasized in this work may find important applications in imaging, sensing, and optical communications.

METHODS

The diameter of the PSHM substrate is 25 mm with a thickness of 3 mm, and the patterned area centered on a glass substrate is 4 mm × 4 mm region. The PSHM is fabricated by using a femtosecond laser at the normal incident writing of spatially varying nanogrooves in a silica glass substrate. The glass substrate is placed on a rotating holder whose rotation speed is controlled by a computer. In the case of intense laser exposure, the silicon glass substrate SiO_2 will decompose into porous glass whose refractive index is associated with the laser intensity. The created uniform birefringent phase retardation is $\vartheta = 2\pi(n_e - n_o)h/\lambda$. Here, h stands for the writing depth and $n_e - n_o$ presents the induced birefringence. The effective ordinary and extraordinary refractive indices are as follows: $n_o = \sqrt{fn_1 + (1-f)n_2^2}$, $n_e = \sqrt{n_1^2 n_2^2/[fn_1^2 + (1-f)n_2^2]}$. Here, f is the filling factor, and n_1 and n_2 represent the refractive indices of the two media which form nanostructured glass slabs. At 633 nm wavelength, the phase retardation ϑ of our sample is π with the writing depth h being about 80 μm, the line width is approximately 30−90 nm, and the filling factor changes in the range of 0.1−0.2. The sample for measuring SEM is prepared by a grinder polisher (Ted Pella Co., Tustin, California). The SEM image of the sample is characterized using a field-emission scanning electron microscope (FE-SEM, Zeiss Sigma 500, Carl Zeiss, Germany).

ASSOCIATED CONTENT

Supporting Information

The Supporting Information is available free of charge on the ACS Publications website at DOI: 10.1021/acsnano.7b07379.

Experimental setup for star images at different wavelengths (PDF)

AUTHOR INFORMATION

Corresponding Authors

*E-mail: zhaowei@ucsd.edu.

*E-mail: hailuluo@hnu.edu.cn.

ORCID

Junxiao Zhou: 0000-0001-6168-8580

Hailu Luo: 0000-0003-3899-2730

DOI: 10.1021/acsnano.7b07379
ACS Nano 2018, 12, 82−88

Author Contributions

[‖]These authors contributed equally to this work.

Notes

The authors declare no competing financial interest.

ACKNOWLEDGMENTS

We thank C. Qiu for a very useful discussion. This work was supported by the National Natural Science Foundation of China (grant nos.11274106 and 11474089) and the China Scholarship Council (scholarship 201606130065)

REFERENCES

(1) Onoda, M.; Murakami, S.; Nagaosa, N. Hall Effect of Light. *Phys. Rev. Lett.* **2004**, *93*, 083901.
(2) Dyakonov, M.; Perel, V. Current-Induced Spin Orientation of Electrons in Semiconductors. *Phys. Lett. A* **1971**, *35*, 459−460.
(3) Hosten, O.; Kwiat, P. Observation of the Spin Hall Effect of Light Via Weak Measurements. *Science* **2008**, *319*, 787−790.
(4) Bliokh, K. Y.; Niv, A.; Kleiner, V.; Hasman, E. Geometrodynamics of Spinning Light. *Nat. Photonics* **2008**, *2*, 748−753.
(5) Qin, Y.; Li, Y.; He, H.; Gong, Q. Measurement of Spin Hall Effect of Reflected Light. *Opt. Lett.* **2009**, *34*, 2551−2553.
(6) Luo, H.; Zhou, X.; Shu, W.; Wen, S.; Fan, D. Enhanced and Switchable Spin Hall Effect of Light near the Brewster Angle on Reflection. *Phys. Rev. A: At., Mol., Opt. Phys.* **2011**, *84*, 043806.
(7) Gorodetski, Y.; Bliokh, K.; Stein, B.; Genet, C.; Shitrit, N.; Kleiner, V.; Hasman, E.; Ebbesen, T. Weak Measurements of Light Chirality with a Plasmonic Slit. *Phys. Rev. Lett.* **2012**, *109*, 013901.
(8) Korger, J.; Aiello, A.; Chille, V.; Banzer, P.; Wittmann, C.; Lindlein, N.; Marquardt, C.; Leuchs, G. Observation of the Geometric Spin Hall Effect of Light. *Phys. Rev. Lett.* **2014**, *112*, 113902.
(9) Slobozhanyuk, A. P.; Poddubny, A. N.; Sinev, I. S.; Samusev, A. K.; Yu, Y. F.; Kuznetsov, A. I.; Miroshnichenko, A. E.; Kivshar, Y. S. Enhanced Photonic Spin Hall Effect with Subwavelength Topological Edge States. *Laser Photonic Rev.* **2016**, *10*, 656−664.
(10) Liu, Z.; Lee, H.; Xiong, Y.; Sun, C.; Zhang, X. Far-Field Optical Hyperlens Magnifying Sub-Diffraction-Limited Objects. *Science* **2007**, *315*, 1686−1686.
(11) Yu, N.; Genevet, P.; Kats, M. A.; Aieta, F.; Tetienne, J.-P.; Capasso, F.; Gaburro, Z. Light Propagation with Phase Discontinuities: Generalized Laws of Reflection and Refraction. *Science* **2011**, *334*, 333−337.
(12) Chen, X.; Huang, L.; Mühlenbernd, H.; Li, G.; Bai, B.; Tan, Q.; Jin, G.; Qiu, C.-W.; Zhang, S.; Zentgraf, T. Dual-Polarity Plasmonic Metalens for Visible Light. *Nat. Commun.* **2012**, *3*, 1198.
(13) Shitrit, N.; Yulevich, I.; Maguid, E.; Ozeri, D.; Veksler, D.; Kleiner, V.; Hasman, E. Spin-Optical Metamaterial Route to Spin-Controlled Photonics. *Science* **2013**, *340*, 724−726.
(14) Lin, D.; Fan, P.; Hasman, E.; Brongersma, M. L. Dielectric Gradient Metasurface Optical Elements. *Science* **2014**, *345*, 298−302.
(15) Bouchard, F.; De Leon, I.; Schulz, S. A.; Upham, J.; Karimi, E.; Boyd, R. W. Optical Spin-to-Orbital Angular Momentum Conversion in Ultra-Thin Metasurfaces with Arbitrary Topological Charges. *Appl. Phys. Lett.* **2014**, *105*, 101905.
(16) Liu, Z.; Li, Z.; Aydin, K. Time-Varying Metasurfaces Based on Graphene Microribbon Arrays. *ACS Photonics* **2016**, *3*, 2035−2039.
(17) Xiao, S.; Wang, J.; Liu, F.; Zhang, S.; Yin, X.; Li, J. Spin-Dependent Optics with Metasurfaces. *Nanophotonics* **2017**, *6*, 215−234.
(18) Monticone, F.; Alù, A. Metamaterial, Plasmonic and Nanophotonic Devices. *Rep. Prog. Phys.* **2017**, *80*, 036401.
(19) Zhao, Z.; Pu, M.; Gao, H.; Jin, J.; Li, X.; Ma, X.; Wang, Y.; Gao, P.; Luo, X. Multispectral Optical Metasurfaces Enabled by Achromatic Phase Transition. *Sci. Rep.* **2015**, *5*, 15781.
(20) Chen, S.; Cai, Y.; Li, G.; Zhang, S.; Cheah, K. W. Geometric Metasurface Fork Gratings for Vortex-Beam Generation and Manipulation. *Laser Photonics Rev.* **2016**, *10*, 322−326.
(21) Zheng, G.; Wu, W.; Li, Z.; Zhang, S.; Mehmood, M. Q.; He, P. a.; Li, S. Dual Field-of-View Step-Zoom Metalens. *Opt. Lett.* **2017**, *42*, 1261−1264.
(22) Yin, X.; Ye, Z.; Rho, J.; Wang, Y.; Zhang, X. Photonic Spin Hall Effect at Metasurfaces. *Science* **2013**, *339*, 1405−1407.
(23) Kapitanova, P. V.; Ginzburg, P.; Rodríguez-Fortuño, F. J.; Filonov, D. S.; Voroshilov, P. M.; Belov, P. A.; Poddubny, A. N.; Kivshar, Y. S.; Wurtz, G. A.; Zayats, A. V. Photonic Spin Hall Effect in Hyperbolic Metamaterials for Polarization-Controlled Routing of Subwavelength Modes. *Nat. Commun.* **2014**, *5*, 3226.
(24) Xiao, S.; Zhong, F.; Liu, H.; Zhu, S.; Li, J. Flexible Coherent Control of Plasmonic Spin-Hall Effect. *Nat. Commun.* **2015**, *6*, 8360.
(25) Liu, Y.; Ling, X.; Yi, X.; Zhou, X.; Chen, S.; Ke, Y.; Luo, H.; Wen, S. Photonic Spin Hall Effect in Dielectric Metasurfaces with Rotational Symmetry Breaking. *Opt. Lett.* **2015**, *40*, 756−759.
(26) Zhang, Y.; Li, P.; Liu, S.; Zhao, J. Unveiling the Photonic Spin Hall Effect of Freely Propagating Fan-Shaped Cylindrical Vector Vortex Beams. *Opt. Lett.* **2015**, *40*, 4444−4447.
(27) Shaltout, A.; Liu, J.; Kildishev, A.; Shalaev, V. Photonic Spin Hall Effect in Gap−Plasmon Metasurfaces for on-Chip Chiroptical Spectroscopy. *Optica* **2015**, *2*, 860−863.
(28) Zhou, X.; Ling, X.; Luo, H.; Wen, S. Identifying Graphene Layers Via Spin Hall Effect of Light. *Appl. Phys. Lett.* **2012**, *101*, 251602.
(29) Bomzon, Z.; Biener, G.; Kleiner, V.; Hasman, E. Space-Variant Pancharatnam−Berry Phase Optical Elements with Computer-Generated Subwavelength Gratings. *Opt. Lett.* **2002**, *27*, 1141−1143.
(30) Shitrit, N.; Bretner, I.; Gorodetski, Y.; Kleiner, V.; Hasman, E. Optical Spin Hall Effects in Plasmonic Chains. *Nano Lett.* **2011**, *11*, 2038−2042.
(31) Luo, W.; Xiao, S.; He, Q.; Sun, S.; Zhou, L. Photonic Spin Hall Effect with Nearly 100% Efficiency. *Adv. Opt. Mater.* **2015**, *3*, 1102−1108.
(32) Zeng, J.; Li, L.; Yang, X.; Gao, J. Generating and Separating Twisted Light by Gradient−Rotation Split-Ring Antenna Metasurfaces. *Nano Lett.* **2016**, *16*, 3101−3108.
(33) Luo, X.; Pu, M.; Li, X.; Ma, X. Broadband Spin Hall Effect of Light in Single Nanoapertures. *Light: Sci. Appl.* **2017**, *6*, e16276.
(34) Zhang, F.; Pu, M.; Luo, J.; Yu, H.; Luo, X. Symmetry Breaking of Photonic Spin-Orbit Interactions in Metasurfaces. *Opto-Electron. Eng.* **2017**, *44*, 319−325.
(35) Ke, Y.; Liu, Y.; Zhou, J.; Liu, Y.; Luo, H.; Wen, S. Optical Integration of Pancharatnam-Berry Phase Lens and Dynamical Phase Lens. *Appl. Phys. Lett.* **2016**, *108*, 101102.
(36) Pancharatnam, S. Generalized Theory of Interference and Its Applications. *Proc. - Indian Acad. Sci., Sect. A* **1956**, *44*, 398−417.
(37) Berry, M. V. The Adiabatic Phase and Pancharatnam's Phase for Polarized Light. *J. Mod. Opt.* **1987**, *34*, 1401−1407.
(38) Hasman, E.; Kleiner, V.; Biener, G.; Niv, A. Polarization Dependent Focusing Lens by Use of Quantized Pancharatnam−Berry Phase Diffractive Optics. *Appl. Phys. Lett.* **2003**, *82*, 328−330.
(39) Pu, M.; Li, X.; Ma, X.; Wang, Y.; Zhao, Z.; Wang, C.; Hu, C.; Gao, P.; Huang, C.; Ren, H.; et al. Catenary Optics for Achromatic Generation of Perfect Optical Angular Momentum. *Sci. Adv.* **2015**, *1*, e1500396.
(40) Beresna, M.; Gecevičius, M.; Kazansky, P. G.; Gertus, T. Radially Polarized Optical Vortex Converter Created by Femtosecond Laser Nanostructuring of Glass. *Appl. Phys. Lett.* **2011**, *98*, 201101.
(41) Hakobyan, D.; Brasselet, E. Left-Handed Optical Radiation Torque. *Nat. Photonics* **2014**, *8*, 610−614.
(42) Biener, G.; Gorodetski, Y.; Niv, A.; Kleiner, V.; Hasman, E. Manipulation of Polarization-Dependent Multivortices with Quasi-Periodic Subwavelength Structures. *Opt. Lett.* **2006**, *31*, 1594−1596.
(43) Ling, X.; Zhou, X.; Yi, X.; Shu, W.; Liu, Y.; Chen, S.; Luo, H.; Wen, S.; Fan, D. Giant Photonic Spin Hall Effect in Momentum Space in a Structured Metamaterial with Spatially Varying Birefringence. *Light: Sci. Appl.* **2015**, *4*, e290.
(44) Goodman, J. W. *Introduction to Fourier Optics*. Roberts and Company Publishers: Greenwood Village, CO, 2005.

DOI: 10.1021/acsnano.7b07379
ACS Nano 2018, 12, 82−88

(45) Aieta, F.; Kats, M. A.; Genevet, P.; Capasso, F. Multiwavelength Achromatic Metasurfaces by Dispersive Phase Compensation. *Science* **2015**, *347*, 1342−1345.
(46) Wang, S.; Wu, P. C.; Su, V.-C.; Lai, Y.-C.; Chu, C. H.; Chen, J.-W.; Lu, S.-H.; Chen, J.; Xu, B.; Kuan, C.-H. Broadband Achromatic Optical Metasurface Devices. *Nat. Commun.* **2017**, *8*, 187.
(47) Jiang, W. X.; Qiu, C. W.; Han, T. C.; Cheng, Q.; Ma, H. F.; Zhang, S.; Cui, T. J. Broadband All-Dielectric Magnifying Lens for Far-Field High-Resolution Imaging. *Adv. Mater.* **2013**, *25*, 6963−6968.

DOI: 10.1021/acsnano.7b07379
ACS Nano 2018, 12, 82−88